Supporting Information: Evaluating the Catalytic Efficiency of Paired, Single-atom Catalysts for the Oxygen Reduction Reaction

Michelle A. Hunter,[†] Julia M. T. A. Fischer,[†,‡] Qinghong Yuan,[†] Marlies Hankel,[†] and Debra J. Searles[*,†,¶]

†*Centre for Theoretical and Computational Molecular Science, The Australian Institute for Bioengineering and Nanotechology, The University of Queensland, Queensland 4072, Australia*

‡ *Data61 CSIRO, Door 34 Goods Shed, Village Street, Docklands VIC, 3008, Australia*

¶*School of Chemistry and Molecular Biosciences, The University of Queensland, Queensland 4072, Australia*

E-mail: d.bernhardt@uq.edu.au

Supporting Data

Table S1: Combined ZPE and entropy corrections for the adsorbed species at 298 K.[1]

Intermediate	$\Delta ZPE - T\Delta S$ (eV)
*OOH	0.40
*OH	0.35
*O	0.02

The DFT calculated energies of O_2 and O-containing species such as peroxy intermediates are known to exhibit large degrees of calculation error. This is due to limitations of DFT's

capacity to correctly describe the ground state of O_2. Following Man et al.,[2] in our approach we limit systematic errors by using the energies of H_2 and H_2O as reference energies and reference to the experimental value of the fuel cell reaction of 4.92 eV. Furthermore, as all the steps in the ORR that produce H_2O can result in either an adsorbed or bound water, we only exclusively calculate the free water case. Additionally, we do not specifically calculate H_2O above the surface as it does not significantly contribute to the energy of the intermediate on the surface and hence the barrier potential dependence of the intermediates. For example, the reaction energy for *OOH was calculated as follows:

$$\Delta E_{^*\mathrm{OOH}} = E_{^*\mathrm{OOH+SF}} - E_{\mathrm{SF}} - (2E_{\mathrm{H_2O}} - \frac{3}{2}E_{\mathrm{H_2}}), \tag{1}$$

This was applied to *OH and *O in a similar fashion. In all cases, multiple initial geometries of the adsorbate were tested for their interaction with the surface. The most stable geometries were used. In Table S1 the combined ZPE and entropy corrections added to each of the intermediates are tabulated.

Table S2: Table of average metal binding energies (E_b) per atom in eV for the systems N6V4 and N8V4, and average cohesive energy (E_coh) for the metal atoms calculated from Kittel.[3]

Pair	E_b (N6V4)	E_b (N8V4)	E_coh [3]
CoCo	5.72	6.69	4.39
CoNi	5.78	6.56	4.42
CoPt	5.86	6.80	5.12
FeCo	5.80	6.61	4.34
FeFe	6.97	6.54	4.28
FeNi	5.75	6.48	4.36
FePt	5.87	6.58	5.06
NiNi	5.92	6.38	4.44
NiPt	6.01	6.61	5.14
PtPt	5.96	6.89	5.84

Table S3: Table of U_{onset} and η for the PSAC systems in V.

Surface	U_{onset} (N6V4)	η (N6V4)	U_{onset} (N8V4)	η (N8V4)
CoCo	-0.09 [a]	1.23	0.86	0.37
CoNi	0.36	0.87	0.88	0.35
CoPt	0.52	0.71	0.93	0.30
FeCo	0.36	0.87	0.63	0.60
FeFe	-0.23 [a]	1.23	0.58	0.65
FeNi	0.18	1.05	0.56	0.67
FePt	0.11	1.12	0.54	0.69
NiNi	0.55	0.68	0.45	0.78
NiPt	0.49	0.74	0.46	0.77
PtPt	0.63	0.60	0.16	1.07

[a] limiting potential in this case was plotted as negative so as to continue the ORR volcano below the x axis. It simply denotes that the reaction is effectively poisoned at $U = 0$ as the *OH adsorption step is is uphill in free energy.

Table S4: Table of the ORR free energy values for the systems N6V4 and N8V4.

Surface	$\Delta G_{^*\text{OOH}}$	$\Delta G_{^*\text{O}}$	$\Delta G_{^*\text{OH}}$
CoCo@N6V4	3.79	0.20	-0.09
CoNi@N6V4	3.74	0.81	0.36
CoPt@N6V4	3.58	1.09	0.57
FeCo@N6V4	3.48	0.19	0.20
FeFe@N6V4	3.08	-0.24	-0.23
FeNi@N6V4	3.50	0.52	0.18
FePt@N6V4	3.35	0.77	0.11
NiNi@N6V4	4.37	1.59	1.16
NiPt@N6V4	4.43	1.89	1.33
PtPt@N6V4	4.29	2.05	1.31
CoCo@N8V4	4.06	2.18	1.07
CoNi@N8V4	4.04	2.12	1.03
CoPt@N8V4	3.99	2.11	1.02
FeCo@N8V4	3.75	1.40	0.63
FeFe@N8V4	3.66	1.35	0.58
FeNi@N8V4	3.67	1.42	0.56
FePt@N8V4	3.60	1.39	0.54
NiNi@N8V4	4.47	3.00	1.46
NiPt@N8V4	4.46	2.58	1.46
PtPt@N8V4	4.76	4.02	2.08

Table S5: Table of magnetic moments (μ_B) in Bohr magnetons (B.M) for the transition metals for the surfaces N6V4 and N8V4.

SF(N6V4)	μ_{M_1}	μ_{M_2}	SF(N8V4)	μ_{M_1}	μ_{M_2}
CoCo	1.22	1.23	CoCo	0.44	-0.45
CoNi	1.21	0.01	CoNi	0.41	0.00
CoPt	-1.32	-0.08	CoPt	0.39	0.00
FeCo	2.44	1.04	FeCo	1.75	-0.50
FeFe	2.24	2.24	FeFe	-1.76	1.77
FeNi	2.49	0.10	FeNi	1.73	-0.02
FePt	-2.63	-0.13	FePt	1.72	-0.01
NiNi	0.00	0.00	NiNi	0.00	0.00
NiPt	0.00	0.00	NiPt	0.00	0.00
PtPt	0.00	0.00	PtPt	0.01	0.01

Determination of the theoretical volcano plot

The oxygen species of the 4e$^-$ ORR pathway have been found to follow linear scaling relationships as they bind similarly to the surface through the O-atom.[4] The free energies calculated in this study were used to calculate the theoretical volcano curve which gives the onset potential as a function of $\Delta G_{*\mathrm{OH}}$. This can be determined by evaluating the relationship between $\Delta G_{*\mathrm{OOH}}$ and $\Delta G_{*\mathrm{OH}}$ which has been proposed from results of numerous studies to be $\Delta G_{*\mathrm{OOH}} = \Delta G_{*\mathrm{OH}} + 3.2$ and has been estimated to have a systematic error of approximately $\pm$ 0.2 eV.[5] As the thermodynamically limiting steps of the ORR are generally found to be either the fourth step $^*\mathrm{OH} + \mathrm{H}^+ + e^- \rightarrow \mathrm{H_2O}$ for strong O-binding species, and the first step $^*\mathrm{O_2} + \mathrm{H}^+ + e^- \rightarrow {}^*\mathrm{OOH}$ for weak binding species, the two sides of the theoretical volcano plot are written as follows:

$$U_1 = \Delta G_{\mathrm{O_2}} - \Delta G_{*\mathrm{OOH}} = -\Delta G_{*\mathrm{OH}} + 1.72\ \mathrm{eV} \tag{2}$$

$$U_4 = \Delta G_{\mathrm{H_2O}} - \Delta G_{*\mathrm{OH}} = -\Delta G_{*\mathrm{OH}} \tag{3}$$

since $\Delta G_{O_2} = 4.92$ eV and $\Delta G_{H_2O} = 0$ eV. Using the data for the systems considered in this study, the relationship between ΔG_{*OOH} and ΔG_{*OH} is $\Delta G_{*OOH} = \Delta G_{*OH} + 3.16$ eV when we fix the slope to be 1, as shown in Figure S1. Therefore, $U_1 = \Delta G_{*OH} + 1.76$ eV. This is plotted on the right side of the volcano in Figure 3.

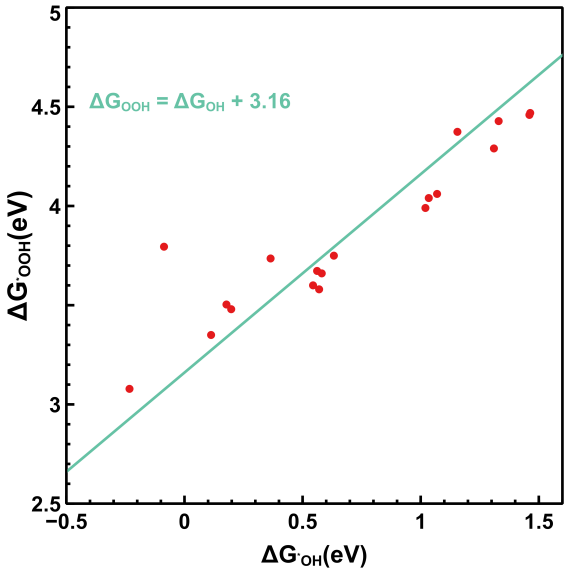

Figure S1: Scaling relations of OH and OOH intermediates. The function obtained by fixing a slope of 1 is shown in green.

These values are close to similar fits obtained for similar graphitic pores with transition metals and within the expected errors.[5,6] However, since the weakly absorbing species are mostly N8V4 pairs, the theoretical line sits underneath the points on the right-hand side of the volcano in Figure 3.

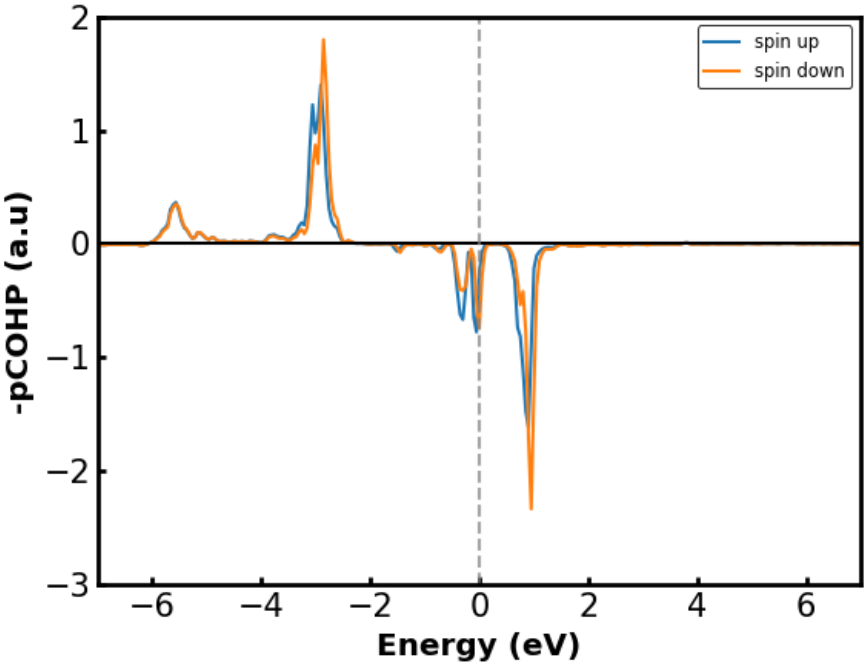

Figure S2: pCOHP of d_{z^2}-p_z interaction of Co-OH of Co in CoPt@N8V4.

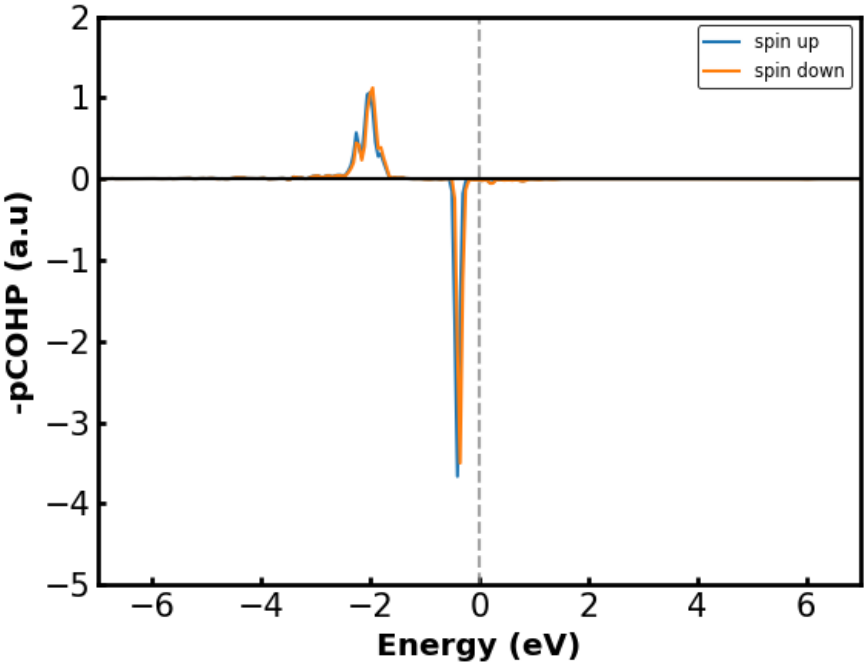

Figure S3: pCOHP of the d_{xz}-p_x interaction of Co-OH in CoPt@N8V4.

References

(1) Fischer, J. M. T. A. Computational Studies of Approaches to Enhance the Catalytic Performances of Graphene and Graphitic Carbon-Nitride Materials. Ph.D. thesis, The University of Queensland, 2018.

(2) Man, I. C.; Su, H. Y.; Calle-Vallejo, F.; Hansen, H. A.; Martínez, J. I.; Inoglu, N. G.; Kitchin, J.; Jaramillo, T. F.; Nørskov, J. K.; Rossmeisl, J. Universality in Oxygen Evolution Electrocatalysis on Oxide Surfaces. *ChemCatChem* **2011**, *3*, 1159–1165.

(3) Kittel, C. *Introduction to Solid State Physics*, 8th ed.; Hoboken, NJ : Wiley, 2005.

(4) Kulkarni, A.; Siahrostami, S.; Patel, A.; Nørskov, J. K. Understanding Catalytic Activity Trends in the Oxygen Reduction Reaction. *Chem. Rev.* **2018**, *118*, 2302–2312.

(5) Christensen, R.; Hansen, H. A.; Dickens, C. F.; Nørskov, J. K.; Vegge, T. Functional Independent Scaling Relation for ORR/OER Catalysts. *J. Phys. Chem. C* **2016**, *120*, 24910–24916.

(6) Calle-Vallejo, F.; Martínez, J. I.; Rossmeisl, J. Density Functional Studies of Functionalized Graphitic Materials with Late Transition Metals for Oxygen Reduction Reactions. *Phys. Chem. Chem. Phys.* **2011**, *13*, 15639–15643.